PHYSICAL REVIEW B VOLUME 15, NUMBER 8 15 APRIL 1977

Surface plasmon dispersion in liquid mercury

Daniel Guidotti and Stuart A. Rice
Departments of Physics and Chemistry and the James Franck Institute, University of Chicago, Chicago, Illinois 60637
(Received 2 July 1976)

The electronic properties of the surface of liquid mercury have been studied from 1 to 6.5 eV via the interaction of the electromagnetic field with the surface plasmons. Our results strongly suggest the existence of an atomic configuration encompassing the outermost two or three atomic layers which is more ordered than the interior. On the basis of model calculations we also postulate a weak, but significant, interaction between the bulk and surface plasmons. The model which we propose here accounts well for our surface-plasmon data and for available ellipsometric and reflectance measurements.

I. INTRODUCTION

Our present understanding of the nature of the surface of a liquid is rudimentary. One of the few robust observations that can be made is the following: Given the atomic structure of matter, it is certain that there exists a transition zone of nonzero width separating the bulk isotropic liquid from whatever medium it contacts. This paper is concerned with the study of the electronic properties of that inhomogeneous distribution of matter near the surface of a liquid metal. That is, how do the transport properties of a liquid metal vary as a function of distance from the surface?

A principal factor inhibiting rapid development of our understanding of the properties of liquid surfaces is the lack of techniques which satisfactorily probe these properties. There are two aspects to this problem. First, most methods of study have response functions that depend on both bulk and surface properties, the contribution to any measurement of the latter usually being much smaller than that of the former. Second, the analysis of experimental data often involves assumptions which lead to distortion or loss of the little information about the surface that the measurement contains. For example, the phase shift and amplitude of reflection of polarized light from a metal depend on the conductivity as a function of depth in the metal. Because the surface transition zone is only a small fraction of the penetration depth of the radiation the "surface contribution" is small relative to the "bulk contribution." Whatever the contribution of the surface zone to the phase shift, etc., it cannot be extracted from a macroscopic analysis of the data based on the use of the Fresnel relations, since these assume that the metal is homogeneous up to a mathematical planar surface. It is imperative, then, that studies of surface properties use both the most sensitive available methodology and a model-free analysis of the data obtained.

A few years ago Bloch and Rice[1] proposed that the available ellipsometric and reflectance spectra of liquid mercury could not be consistently interpreted if the existence of a transition zone at the liquid surface was neglected. For liquid mercury the normal-incidence reflection spectrum, via Kramers-Kronig inversion, gives values for the real and imaginary parts of the dielectric function which differ from those obtained from ellipsometry.[2-4] Stated another way, and avoiding use of Kramers-Kronig inversion of reflectance data, the optical constants inferred from the ellipsometric data imply a normal incidence reflection spectrum in disagreement with that observed. The discrepancy is real; data taken in many laboratories and in an apparatus designed to permit ellipsometric and reflectance measurements on a common surface confirm the observations.[5] Bloch and Rice showed that if the conductivity as a function of distance from the surface increases continuously from the bulk value to a maximum in the surface region before decaying smoothly to zero outside the metal, the disparate ellipsometric and reflection spectra can be reconciled with considerable accuracy. This model of the surface conductivity also accounts for the unpolarized reflection spectrum at oblique incidence.[1] The most important feature of the model, and the one primarily responsible for its success, is the existence of the peak in the conductivity at the surface.

Lang and Kohn[6] have studied the electron density distribution at the surface of a model metal in which the positive-ion distribution is replaced by a positive jellium with uniform density up to a plane surface, at which the positive density falls abruptly to zero. They find that there is a transition region between bulk metal and vacuum in which the electron density has a damped oscillatory character on the bulk side, reminiscent of Friedel oscillations, and falls smoothly to zero on the

vacuum side. In a metal for which $r_s = 5$, the electron density reaches a peak in the transition region which is about 13% above the bulk density. Note that in this model no account is taken of electron-ion interactions, or ion-ion interactions, and the positive and negative charge distributions are not allowed to self-consistently relax, as must occur in a real metal. The model thereby neglects any surface structure which results from said relaxation.

The theoretical analysis by Lang and Kohn, supplemented by qualitative application of the Hellman-Feynman theorem,[7] suggests that the inference of structure in the surface transition zone is worthy of more detailed investigation. Two caveats must be mentioned. First, the Bloch-Rice analysis refers to a conductivity profile and the Lang-Kohn analysis to an electron density profile. The relationship between these two profiles includes system parameters such as the effective electron mass and relaxation time due to scattering, hence there is not a one-to-one correlation between the amplitudes of the two profiles. Second, examination of the parameters of the inferred conductivity profile leaves one with an uncomfortable feeling. The thickness of the transition zone (about two atomic layers) seems sensible, but the suggested surface conductivity, of order twelve times the bulk conductivity in the case of a delocalized electron model,[1,5] appears implausibly large. Even the use of a skewed profile, which allows for a metal to nonmetal transition on the low density side of the transition region, hence some localized electronic states, has a maximum surface conductivity about five times the conductivity of the bulk metal. The extent to which a high surface conductivity is consistent with available optical and structural information will be discussed in Sec. V.

The inferences and caveats described underscore the need for new and different experimental and theoretical studies of liquid surfaces. Lemberg, Rice, and Guidotti[8-10] showed that surface-plasmon dispersion is sensitive to the properties of the transition region. When taken together with ellipsometric and reflectance data the information available is sufficient to impose real restrictions on models of the conductivity profile at a liquid-metal surface. In this paper we report a quantitative study, by the method of attenuated total reflection[11] (ATR), of the surface-plasmon dispersion of liquid mercury. These data, together with reflectance and ellipsometric data, are compared with the predictions of several models of the conductivity profile. We find that a model which is consistent with all the observations has the following features:

(i) In the interior of the metal the conductivity is adequately characterized by a single relaxation time τ_b and an effective mass close to the free-electron mass. This is consistent with the properties defined by thermal excitation near the Fermi energy, e.g., Hall effect measurements in liquid mercury. (ii) The outermost two or three atomic layers have a somewhat more ordered structure than does the bulk liquid. (iii) As a consequence of (ii) there is a peak in conductivity at the surface. The magnitude of the peak conductivity is comparable to the conductivity of polycrystalline Hg. (iv) There is a nonvanishing surface-plasmon–bulk-plasmon interaction which leads to an additional channel for decay of the surface plasmon.

Predictions derived from the described semiempirical model of the surface properties of liquid Hg are in good agreement with the experimental data except for the shape of the ATR resonance. None of the models we or others have considered yield a good fit to the shape of the ATR resonances.

II. EXPERIMENTAL DETAILS

Our investigation of the dispersion relation for surface plasmons in liquid Hg is based on the method of ATR, introduced for this purpose by Otto.[11] The physical principle on which this method is based is as follows.

The electromagnetic field associated with the surface-plasmon oscillations at a smooth metal surface is nonradiative. That is, it is exponentially damped along the direction normal to the metal surface, while propagating parallel to the surface. At a smooth surface it is, therefore, not possible for a plane electromagnetic field to interact with the surface charge oscillations. Furthermore, the propagation vector for surface plasmons is always larger than the propagation vector of photons in the medium contacting the metal.[9,11-14] When total reflection of plane waves occurs at an interface between two dielectric media (medium A has a higher index of refraction than medium B), it can be shown that an evanescent field exists about the interface.[15] The field propagates along the boundary but decays exponentially into the medium of smaller index of refraction (medium B). It, therefore, has the same form as the surface plasmon field. To affect coupling between the two fields, and, therefore, optical coupling, the propagation vector of the evanescent wave must match that of the surface plasmon. The ATR technique accomplishes this by bringing a totally reflecting boundary in proximity to a metal surface. The propagation vector of surface plasmons depends on the index of refraction of the contact medium, in this case n_B. The propagation vector of the evanescent field depends on the index

of refraction of medium A and is given by $k = n_A(\omega/c)\sin\theta$, where θ is the angle of incidence, ω is the frequency of incident radiation, and c is the speed of light in vacuum. Optical coupling to surface plasmons is effected by varying θ to match the evanescent field to the surface plasmon field. For a more thorough description of the ATR method see Refs. 9, 11, and 12–14.

In this section we describe the many practical details which define our exploitation of the ATR technique. Our ATR optical couplers consisted of prisms with a thin layer coating of LiF or NaF on the face that contacted the liquid. For photons in the energy range 1.2–3.5 eV the prisms were made of a high index of refraction glass, IRG-2, and have surfaces flat to $\frac{1}{4}$ wave in the visible. For photons in the energy range 2.5–6.5 eV the prisms were made of single-crystal quartz with the optic axis oriented perpendicular to the plane of incidence so that the TM polarization of the incident radiation would not be altered by rotation. These prisms are finished to $\frac{1}{4}$ wave in the visible. For both glass and quartz prisms the angles are known to ±1 min of arc.

The thin-film LiF and NaF coatings were prepared anew for each experiment; the thicknesses were chosen to be appropriate to the wavelength ranges of the experiments. Deposition of the films was carried out by thermal evaporation from a tungsten boat in a vacuum of about 3×10^{-8} Torr. The NaF used was supplied by the J. T. Baker Co. in powder form and had a stated purity of 99.9% with the following contaminants: carbonates (0.05 mole%), fluorosilicates (0.02 mole%), sulfates (0.01 mole%) and a trace of heavy metals (0.001 mole%). The LiF used was obtained from Karl Lambrecht, Inc. in the form of discarded chips from a parent single crystal; it was of optical purity.

Following deposition the spacer films were annealed at ~100 °C and 5×10^{-8} Torr for no less than 8 h. The coated prisms were then transferred to a dessicator and stored under partial vacuum (~$\frac{1}{3}$ atm). To minimize the adsorption of environmental moisture by the LiF and NaF films during the sample preparation, a handling system was devised whereby the prism coupler was exposed to the room atmosphere for no more than 4 min. We have qualitative evidence that moisture contamination did not influence our experiments unless the prism coupler was exposed to the environment for more than 6 h. It was found to be inadvisable to store a prism coupler in the dessicator for more than two days. After this period it often became difficult to obtain good optical contact between the liquid Hg and the NaF or LiF film. In the usual case a newly prepared prism coupler was mounted in a cell for an experiment in 2 h or less. An actual experiment lasted about 36 h. The high degree of reproducibility in our data is evident from a comparison of data taken at the same wavelength both at the beginning and at the end of the 36 h period. The two sets of data are virtually indistinguishable. Data which did not show this degree of reproducibility were assumed to be indicative of a vacuum leak and subsequent contamination, and were discarded. The mercury used was triply distilled 99.9995% pure and supplied by D. F. Goldsmith Chemical and Metal Corp.

To use the data obtained in an ATR measurement one must know the thickness and refractive index of the spacer layer. The film thickness was monitored with an overall uncertainty of 3% by a crystal-quartz oscillator (International Crystal Mfg. Co., Inc.). The refractive indices of the films were measured in the following way. A hexagonal prism with unpolished back surface (to eliminate internal reflection) was used as the test substrate. Half of the polished front surface was coated with a sample film and the Brewster angle at the air-film interface was determined by a null measurement technique derived from a discussion in Heaven's monograph.[16] At the Brewster angle the TM radiation incident on the air-film interface has zero reflection amplitude, hence is totally transmitted. The transmitted beam is, however, partially reflected at the film-prism interface. Therefore, a measurement of the difference in intensities, as a function of angle, of light reflected from the coated and uncoated portions of the prism substrate is a very sensitive null determination of the Brewster angle. In our application of this method the overall error in angular measurement was ±1.4 min of arc, corresponding to ±0.13% uncertainty in the refractive index of the film. The NaF films were found to have a refractive index (1.4–1.5)% lower than that of a NaF single crystal, and to have the same dispersion [Fig. 1(b)]. The LiF films had a refractive index about 3% lower than that of the single crystal, and the dispersions of the film and single-crystal refractive indices are different [Fig. 1(a)]. The index of refraction of NaF films was found to not vary significantly with thickness over the range 800–1700 Å, nor was there any variation noted amongst the many depositions made at the same thickness (825 Å) but with slightly different rates of deposition. In contrast, the properties of the LiF films are sensitive to rate of deposition and, somewhat less so, to thickness of deposit.

The sample cell used (Fig. 2) was spark cut from a stainless-steel block. The window of the cell was the prism coupler itself, affixed with an epoxy cement. At first Perkin-Elmer Vac-

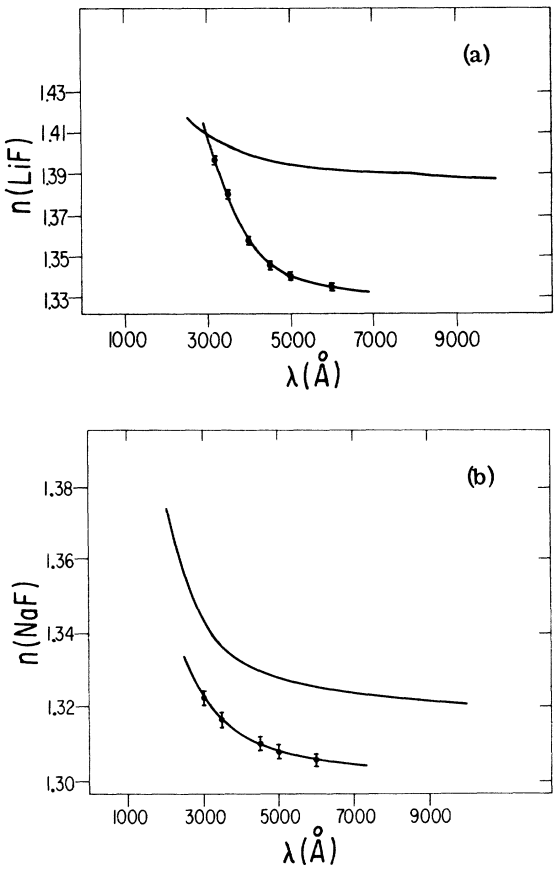

FIG. 1. (a) Index of refraction of LiF. In the upper curve we show the single-crystal value obtained from standard tables. The index of refraction which we measure for a particular film is shown in the lower curve. Of course, the film index of refraction varies with rate of deposition and film thickness. (b) Index of refraction of NaF. The single-crystal table value is shown in the upper curve. The lower curve represents a typical film index of refraction reproducible, within experimental error, for slightly different evaporation parameters.

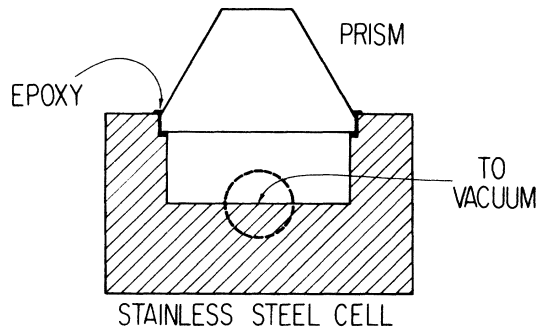

FIG. 2. Schematic diagram of sample cell. The prism window is affixed by epoxy.

Seal epoxy was used, but later Devcon "5-minute" epoxy was employed as it proved easier to remove (and retrieve the prism) at the end of an experiment. A Pyrex-to-stainless-steel connector served to join the cell to a vacuum and distillation line constructed entirely of Pyrex glass except for Teflon stopcocks with viton O rings.

An amount of mercury was vacuum distilled into a reservoir from which the sample cell was filled to half capacity under vacuum. Prior to each distillation the system was flushed with H_2 and, before complete removal of the H_2, a gaseous discharge was generated with a Tesla coil to further scavenge residual O_2. The system was then baked and pumped down typically to 3×10^{-6} Torr by a liquid N_2 trapped Hg diffusion pump. The partially filled cell was removed from the line via a glass pinch off seal. All measurements were made on liquid-Hg samples in equilibrium with Hg vapor.

The disperser in our surface plasmon spectrometer is a McPherson 218, 0.3-m monochromator. From 1.2 to 3.4 eV the light source was a 500-W tungsten-halogen lamp with quartz envelope, and from 2.7 to 6.5 eV a McPherson 630 Hinteregger discharge lamp operated with H_2. An all mirror collimator was constructed. This collimator collects the divergent light from the monochromator and converts it to a beam with full (lateral) angular divergence of 18 sec of arc for a 25-μm monochromator slit. The design, which is illustrated in Fig. 3(a), utilizes a double pass light path and an off-axis parabolic mirror. In the first pass the parabaloid acts as a collector which focuses the slit image of the monochromator at its own focal point via an arrangement of plane mirrors. Collimation is effected on the second pass of the light, which then emerges as a rectangular beam 0.7 cm $\times$ 1.5 cm at a distance 750 cm from the mirror. The divergence of this beam in the vertical direction is about 40 min of arc. This vertical divergence is a consequence of the large monochromator exit-slit height (5 mm) and does not affect the angular resolution in our experiments.

The collimated light is polarized, depending on the wavelength, by a Glan-Taylor prism or a MgF_2 Rochon prism. A schematic representation of the experimental arrangement is shown in Fig. 3(b).

To minimize systematic error a double beam optical system was employed. The sample cell, which was kinematically mounted on a half angle drive goniometer (Societe Genevoise de Physique), was used half-filled. A mirror beam deflector was used to direct light from the upper empty portion of the cell to one phototube, and light from the lower filled portion of the cell, to a second phototube. The two phototubes were mounted pig-

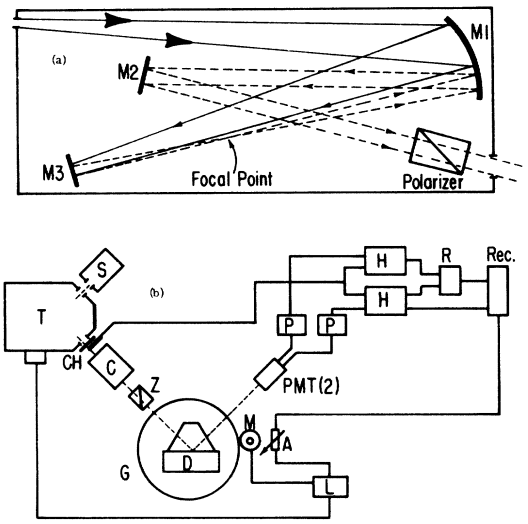

FIG. 3. (a) Mirror collimation. Divergent light incident on the off axis parabolic mirror $M1$ is focused at a point which is brought at the focal point of $M1$ by plane mirror $M3$. Upon second reflection from $M1$ light emerges as a parallel beam which is directed, by plane mirror $M2$, to the polarizer and sample. (b) Block diagram of our experimental arrangement. The solid lines indicate electrical connections, while the dashed lines represent the light path. S-light source, T-monochromator, CH-chopper, C-mirror collimator, Z-polarizer, G-goniometer, D-sample cell, M-synchronous motor, A-microswitch angle marker, L-scanning logic, PMT (2)-two photomultiplier tubes mounted piggy-back, P-preamp for each PMT, H-lock-in amplifier, R-ratiometer, Rec.-Recorder.

gy-back on the detector arm, which rotates at twice the rate of the sample table so as to maintain the specular reflection configuration. A synchronous motor provided the goniometer drive. Amperex 150 CVP infrared sensitive $S-1$ type tubes and EMI 6256QS tubes were used as required. The signal from each phototube was directed to a separate PAR HR8 lock in amplifier, with the modulating signal obtained from a 200-Hz tuning fork beam chopper (Bulova CHI-5A) mounted on the exit slit of the monochromator. The output from each amplifier was then fed into an analog ratiometer built around a Function Modules 540L chip.

The accuracy of the experiment depends on the measurement of the angle at which the minimum in reflectance occurs, and on the intensity of reflected light. The goniometer used, although 50 years old, gave settings reproducible to 4 sec of arc. The ratio of intensities of light reflected from the filled and unfilled portions of the cell was calibrated using the large-angle reflectivity ratio, which must approach unity. The relative phototube gains were adjusted so that unit ratio was obtained at very large angle of incidence. An error in the reflected intensity no greater than 0.5% in the visible, and 2–3% in the ultraviolet, is inherent in this normalization. In addition a slight migration of the reference and sample beams across the faces of the respective phototubes introduces an additional error of (0.5 to 1)% at very large and very small angles. The beams wander because the prism coupler defines an effective plane of reflection which moves across the axis of rotation as the angle of incidence is varied. As a check on the calibration the reflection of TE radiation was measured. To within the noise level (less than 1%) we obtained a constant ratio of intensities for all angles greater than the prism-spacer critical angle. This is expected because of lack of interaction of TE radiation with surface collective modes of the electron gas. Finally, the rated accuracy of the function chip in the ratiometer is 0.1% over two decades of the ratio measured. In practice we found the accuracy to depend on the level of the reference signal which generates the divisor. For reference signal (divisor) levels between 9 and 10 V the measured precision was found to be 0.15% over $1\frac{1}{2}$ decades but the precision decreased as the divisor signal level decreased, and reached 1.6% when it was 5 V. In all our measurements the divisor level was kept between 8 and 10 V, yielding an estimated ratiometer induced error of 0.8%. It is important to note that the magnitude of the divisor is the only determining factor in the accuracy of the ratiometer and, therefore, small beam intensities, as at a resonance minimum, can be measured as accurately as high intensities over the range encountered in our experiments provided the divisor is large enough. This is accomplished by opening or closing the monochromator slit as needed. Stability for both high and low signal beam intensities is important to ensure that the resonance minimum is not artificially shifted by ratiometer drift.

III. OBSERVATIONS

We display, in Fig. 4, the surface-plasmon dispersion for liquid Hg in contact with a film of NaF for energy range 1.1–2.5 eV; for better resolution the dispersion curve is divided in two parts. Dots represent experimental points, and the heavy solid line is an extrapolated fit to these points. The uncertainty in k, which comes from the uncertainty in locating the angle at which resonance absorption is maximum, is everywhere smaller than the dots representing experimental data. Error bars are therefore not shown. The higher-energy portion of the dispersion curve, 3 to 4.5 eV, is displayed in Fig. 5. For improved resolution, we divide this

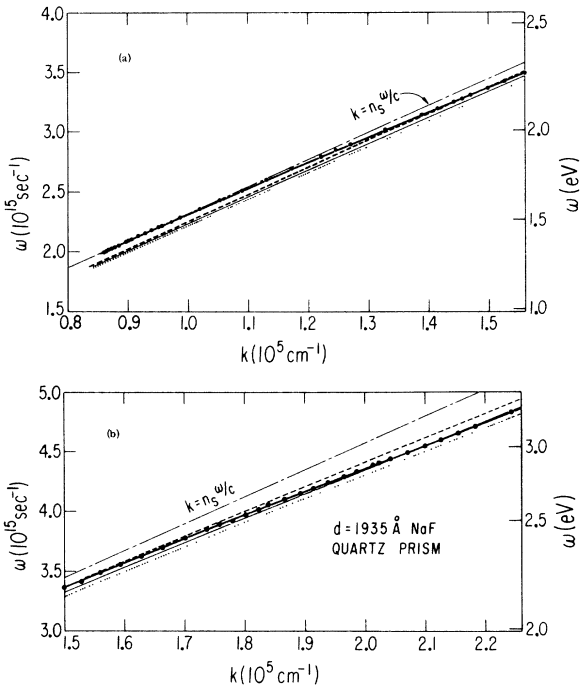

FIG. 4. Surface-plasmon dispersion of liquid mercury in contract with a NaF film deposited on the base of a quartz prism. The curve extends from 1 to 3 eV. The behavior of (SS and LK), GR and BR models are displayed by the dotted, light solid, and dashed lines, respectively. The heavy solid line is an extrapolated fit to experimental points. The long dash-dot line represents the dispersion of plane waves in the NaF film.

curve into sections. The open circles are experimental points. Again, for the lower sections of this curve we do not show error bars as these are smaller than the circles themselves. The heavy solid line is fit to the experimental points. From the data shown we estimate[17] the limiting ($k \to \infty$) surface-plasmon energy to be 4.7 ± 0.2 eV. This value is close to, but less than, the normal-mode surface-plasmon frequency which is obtained by equating the metal dielectric function to the negative square of the index of refraction of the contact medium. From Wilson and Rice[18] we estimate the surface-plasmon frequency to be 5.2 ± 0.1 eV for $n(\mathrm{NaF}) = 1.35$. Krauss and Gomer[19] in an electron energy loss experiment, find a surface-plasmon frequency of 5.4 ± 0.1 eV in the presence of a contact medium with index of refraction of 1.4. We should point out that, whereas these latter values correspond to pure surface-plasmon oscillations (longitudinal), in an ATR experiment one observes a hybrid mode strongly interacting with the electromagnetic field. The radiative decay channel present in this configuration should account for the somewhat lower value we observe for the surface-plasmon frequency. Note that near this limiting value the dispersion curve "bends back," which behavior is characteristic of damped collective oscillations of the electron gas.[20,21] The indicated scatter in the data is a consequence of the flateness of the response function near the limiting surface-plasmon energy. As this energy is approached $\mathrm{Re}\sigma(\omega)/\mathrm{Im}\sigma(\omega) \to 0$, and the radiative damping increases dramatically with the consequence that the absorption resonance becomes very broad and shallow (the real part of the surface-plasmon momentum becomes small relative to the imaginary part and the plasma oscillations become poorly defined energetically).

Finally, in Fig. 13 are shown the shapes of resonance absorption of TM radiation by the surface plasmons. The minimum position depends upon the index of refraction of the spacer film, as well as on the intrinsic properties of the metal. The absorption intensity is determined, in large part, by the radiative coupling through the spacer, which depends on the ratio λ/d; λ is the wavelength of incident radiation in the prism, and d is the spacer thickness. Absorption resonances are deeper and narrower when $\lambda/d \approx 1.5$.

In addition to the experimental data, there are several different curves shown in Figs. 4, 5, and 13. These represent the surface-plasmon dispersion curves predicted by different models of the conductivity profile; they will be discussed in Sec. IV.

IV. ANALYSIS OF MODELS

A. General remarks

The optical constants of a metal are frequently obtained from a Kramers-Kronig inversion of the near normal incidence reflection spectrum. At normal incidence, the reflectance from an isotropic metal is determined by the square of the modulus of the Fresnel reflection coefficient

$$R_s = R_p = |r_s|^2 = |r_p|^2 = R\,, \tag{1}$$

$$r_s = r_p = (n - n_0)/(n + n_0) = \rho_s e^{i\delta_s} = \rho_p e^{i\delta_p} = \rho e^{i\delta}\,, \tag{2}$$

where n and n_0 are the (complex) refractive indices of the metal and the contact medium, $\rho_{s,p}$ is the (real) amplitude of the reflected wave for unit incident amplitude and $\delta_{s,p}$ is the phase change at the surface. The subscripts s and p refer, as usual, to waves polarized perpendicular to and in the plane of incidence, respectively. Then

$$\ln\rho(\omega) = \frac{2}{\pi} P\int_0^\infty \frac{\omega'\delta(\omega') - \omega\delta(\omega)}{\omega'^2 - \omega^2}\, d\omega'\,, \tag{3}$$

$$\delta(\omega) = \frac{2\omega}{\pi} P\int_0^\infty \frac{\ln\rho(\omega') - \ln\rho(\omega)}{\omega'^2 - \omega^2}\, d\omega'\,. \tag{4}$$

Evaluation of $\rho(\omega)$ and $\delta(\omega)$ permits determination of ϵ_1 and ϵ_2 via Eqs. (1) and (2) and the definition

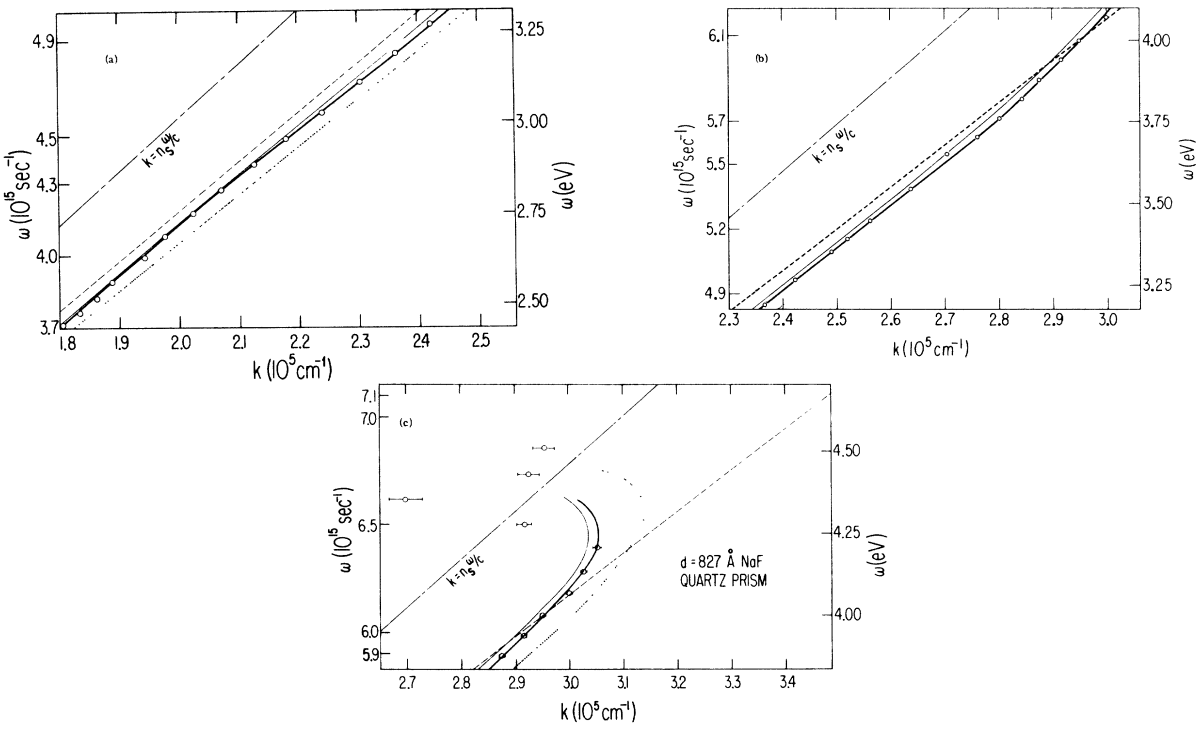

FIG. 5. Higher-energy portion of the surface-plasmon dispersion curve. Again mercury is in contact with a NaF film at the base of a quartz prism, and the predictions of the four models we have considered are represented as in Fig. 4. SS and LK predict very nearly the same dispersion curve and are both represented by the dotted line.

$$n^2=\epsilon\equiv\epsilon_1+i\epsilon_2\,. \tag{5}$$

To obtain the optical constants of a metal from a Kramers-Kronig inversion of the normal incidence reflection spectrum that spectrum must be known over the whole frequency domain, either from experiment or extrapolation. An alternative methodology, which avoids the difficulty of requiring knowledge over the entire frequency domain, is ellipsometric spectroscopy. Because an ellipsometric measurement at any one frequency yields both the ratio of reflection coefficients for radiation with s and p polarizations, $\rho\equiv\rho_p/\rho_s=|r_p|/|r_s|$, and the difference in phase change on reflection of the p and s polarized radiation, $\Delta\equiv\delta_p-\delta_s$, there are sufficient data to determine both the real and imaginary parts of the dielectric function:

$$\epsilon_1(\omega)=n_0^2\sin^2\theta\times\left(1+\tan^2\theta\frac{\cos^2 2\psi-\sin^2 2\psi\sin^2\Delta}{(1+\sin 2\psi\cos\Delta)^2}\right), \tag{6}$$

$$\epsilon_2(\omega)=n_0^2\sin^2\theta\left(\frac{\tan^2\theta\sin 4\psi\sin\Delta}{(1+\sin 2\psi\cos\Delta)^2}\right), \tag{7}$$

where $\tan\psi=\rho$ and θ is the angle of incidence of the radiation on the metal.

It is now important to note that Eqs. (2), (6), and (7) refer to a particular model of the surface of the metal. To be specific, in both cases the interaction of radiation with the metal is analyzed under the assumption that the bulk properties are homogeneous up to a surface plane at which they discontinuously change to the properties of the contact medium. The dielectric function obtained using these equations is, therefore, intimately related to this particular model and it is inconsistent to base detailed conclusions about the structure of the surface-transition region on the dielectric function obtained in such a fashion. We have already noted that, by virtue of the atomic nature of matter, there must be a surface-transition zone wherein the properties of the metal are different from the bulk properties. The contribution of this transition zone to the interaction between radiation and the metal cannot be obtained from Eq. (1)–(7). In what follows we bypass this problem by comparing model predictions directly to ellipsometric, reflectivity, and surface-plasmon dispersion data. That is, we compute the amplitude of the reflection coefficients, change of phase and surface-plasmon dispersion for an inhomogeneous conductor, using different models for the inhomogeneity, and compare these computations with the observed values of the normal incidence reflectivity, ρ and Δ, and the surface-plasmon dispersion and absorption line shape.

B. Definition of models

It has been amply demonstrated that, for energies well below the interband transitions, the conduction electrons in liquid Hg are adequately represented by the nearly-free-electron model.[1,22,23] The characteristic feature of the nearly-free-electron model is the existence of a relatively weak ionic pseudopotential which generates quasi-elastic scattering between nearly plane-wave states, hence the electronic transport properties can be calculated from the Boltzmann equation. One finds that the frequency-dependent conductivity is

$$\sigma(\omega) = \sigma_0/(1+i\omega\tau) \ , \tag{8}$$

$$\sigma_0 = ne^2\tau/m^* \ , \tag{9}$$

with m^* the electron effective mass, τ the relaxation time, and n the electron density.

We refer to the traditional model, in which the properties of the metal are uniform up to the surface plane, at which they abruptly change, as the sharp-surface model [(SS, Fig. 6(a)]. The response of the SS model to an external field is given by the nearly-free-electron theory mentioned above. For liquid Hg, with two conduction electrons per ion core, m^* is very close to the free electron mass. Then the dc conductivity, which is $\sigma_0 = 9.35\times10^{15}$ sec^{-1}, gives $\tau = 0.454\times10^{-15}$ sec. We shall refer to these as bulk values, and use the subscript b to denote them (σ_{0b}, τ_b).

As already noted, the main feature of the model proposed by Bloch and Rice [BR, Fig. 6(b)] is the inclusion between the bulk and contact (e.g., vapor) phase of a transition region. The conductivity rises smoothly from the bulk value to a maximum in the transition zone before decaying to zero on the vacuum (or contact) side of the interfacial region. In symbols, BR assume that

$$\sigma(w) = [w/(1+w)][\sigma_b + \sigma_s/(1+w)] \ , \tag{10}$$

$$w \equiv \exp(2\pi z/\Delta_{BR}) \ , \tag{11}$$

where Δ_{BR} is a measure of the width of the transition zone, σ_b is the bulk conductivity and σ_s determines the magnitude of the conductivity in the

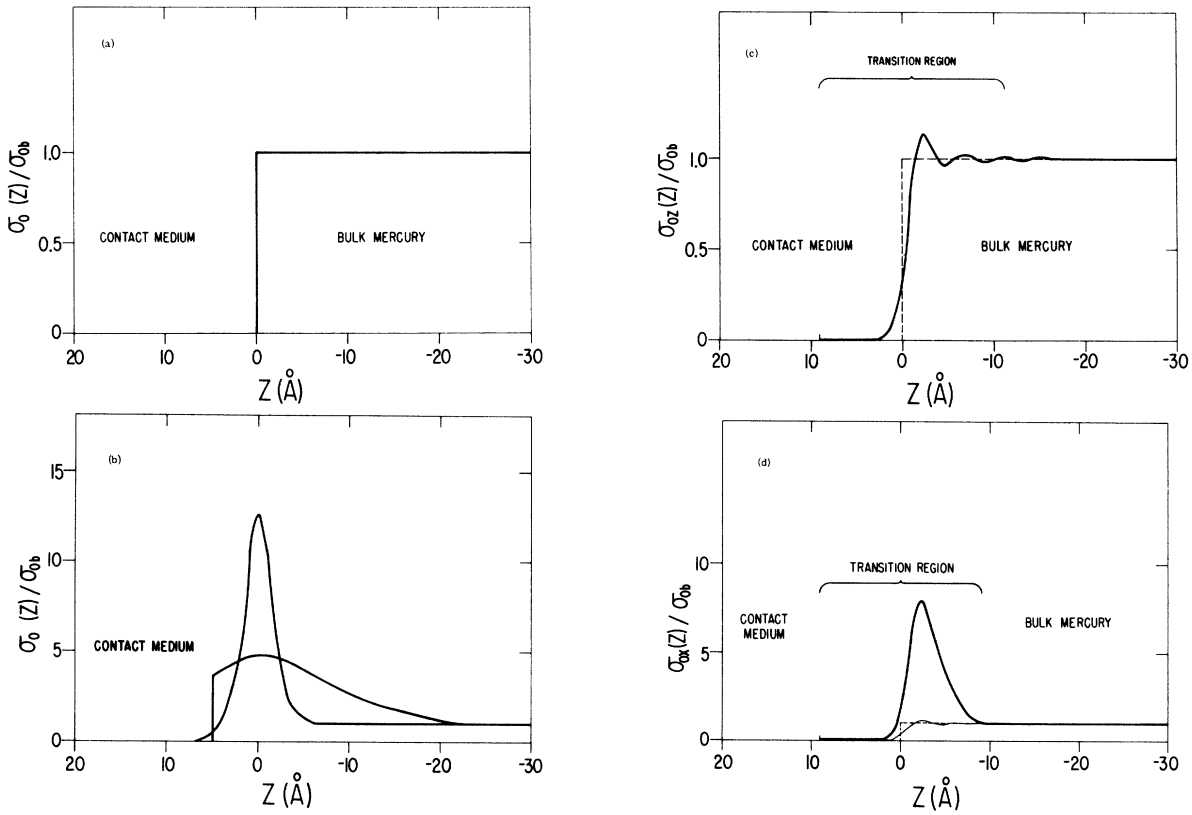

FIG. 6. (a) Conductivity profile of the Drude sharp surface (SS). (b) dc conductivity profile for the two BR models. The lower curve shows the functional dependence of the skewed profile (here we have taken $\tau_b = \tau_s$). The discontinuity is due to the metal-to-nonmetal transition. The upper curve represents the dc conductivity of the delocalized profile. (c) The dc conductivity corresponding to the Lang-Kohn electron density at a jellium surface. Of course, this is also the dc conductivity component perpendicular to the surface in the GR model. The ion density is displayed by the dashed curve. (d) The component of the dc conductivity parallel to the surface in the GR model. The light solid curve is the perpendicular component, $\sigma_{oz}(z)$, and the dashed curve is the ion density.

transition zone. Note that in this model the conductivity is a scalar function, hence isotropic at any given point. BR took the frequency dependence of $\sigma_{s,b}$ to have the form of Eq. (8). A modest generalization of (10) uses different widths, Δ^c_{BR} and Δ^b_{BR}, for the contact and bulk sides of the transition region. In this generalized model σ_s was taken to have the form (8) on the bulk side of the conductivity maximum and the form

$$\sigma_s(\omega) = i\sigma_{0s}\omega/[(\omega_0^2 - \omega^2)\tau_s + i\omega] \tag{12}$$

on the contact medium side when the conductivity has decreased to $0.7\sigma_{0\max}$ where $\sigma_{0\max}$ is the peak conductivity in the transition region. The form (12) is characteristic of localized states, hence its adoption corresponds to postulation of a metal-nonmetal transition on the contact medium side of the transition zone. To fit the then available data Bloch and Rice used $\sigma_{0s} = 17\sigma_{0b}$, $\tau_s = 0.9\tau_b$, $\hbar\omega_0 = 0.8$ eV, $\Delta^b_{BR} = 31.42$ Å, $\Delta^c_{BR} = 6.28$ Å for the asymmetric profile. Using the form (10) BR required $\sigma_{0s} = 48\sigma_{0b}$, $\tau_s = 0.9\tau_b$, and $\Delta = 6.28$ Å. Note that, by virtue of the form of Eq. (10), σ_{0s} is *not* the surface conductivity. In fact the maximum value of the conductivity in the transition zone is about $5\sigma_{0b}$ for the asymmetric generalized BR profile and $12\sigma_{0b}$ for the simple form in Eq. (10).

As shown clearly by Lang and Kohn, a positive jellium with uniform charge density up to a planar surface at which the positive charge density drops to zero supports an oscillatory electron density. It is interesting to see how the existence of such electron density oscillations influence the optical properties of the metal. We associate a dc conductivity with the calculated electron density, taking that conductivity to be a scalar function and defining its magnitude by the ratio of local to bulk densities multiplied by the bulk dc conductivity. We denote this model LK (Lang-Kohn) [Fig. 6(c)].

Finally, we consider a model which, we believe, contains the essential elements of any satisfactory description of the surface transition zone of liquid Hg. These are (i) a peak in conductivity at the surface, (ii) anisotropy of the surface conductivity, i.e., a larger conductivity parallel to the surface than normal to it, and (iii) a bulk plasmon-surface plasmon interaction. The variation of conductivity with position in this model, denoted GR (Guidotti-Rice), is shown in Fig. 6(d). We assume that whatever the form of the ion core distribution near the surface it will support static oscillations in the electron density, and we approximate all but the largest of these by taking over the form calculated by Lang and Kohn. The available data force us to treat the outermost oscillation in electron density—converted to an oscillation in conductivity—differently. We assume that the conductivity parallel to the surface is enhanced in the transition zone, and we take this enhancement to have a Gaussian profile in planes parallel to the surface. The full width at half height of the Gaussian conductivity peak is 6.7 Å, and it coincides with the first peak in the Lang-Kohn electron density profile. However, we do not argue that the excess conductivity implies a one-to-one excess electron density. Instead, as will be argued later, we believe that partial ordering of the outermost layers of the surface changes the effective mass of the electron, and the scattering rate, so as to produce a conductivity peak with very modest changes in the electron density. Note that in this model the conductivity in the surface region is anisotropic. In the direction normal to the surface the conductivity is taken to scale with the Lang-Kohn electron density, which is different from the component of conductivity parallel to the surface just described. In symbols, the GR model assumes that

$$\sigma_x(z, \omega = 0) = \sigma_y(z, \omega = 0) = \sigma_b(\omega = 0)(\rho(z)/\rho_b)_{LK}(1 + Ae^{-(z-z_0)^2/\eta^2}), \tag{13}$$

$$\sigma_z(z, \omega = 0) = \sigma_b(\omega = 0)\left(\frac{\rho(z)}{\rho_b}\right)_{LK}, \tag{14}$$

and for the scattering relaxation time,

$$\tau(z) = \tau_b(1 + Be^{-(z-z_0)^2/\eta^2}), \tag{15}$$

where $(\rho(z)/\rho_b)_{LK}$ is the normalized electron density calculated by Lang and Kohn for a metal with $r_s = 5$. The parameters of the Gaussian form are $\eta = 0.3$ Å^{-1}, $Z_0 = 2.31$ Å, $A = 6$, and $B = 0.25$.

There remains to be discussed one more important aspect of the GR model. The studies by Wilson and Rice show that, because of interband transitions at 8 eV and 10 eV, the bulk plasmon resonance in liquid Hg is displaced downward from the free-electron value $\hbar\omega_p = 10.6$ to 6.9 eV. Moreover, because of a high scattering rate, line broadening in mercury can be rather substantial. A measure of this broadening is the half width at half maximum of the Drude component of $\epsilon_2(\omega)$, which we estimate, from Wilson and Rice, to be 1.6 eV. In Fig. 7, we show the calculated surface-plasmon absorption resonance, near the surface-plasma frequency, as a function of energy for fixed angle of incidence. The half width at half minimum (measured from the low-frequency limit) is 1.4 eV. It is to be expected that, because of this line broadening, residual interactions will lead to a coupling of surface and bulk plasmons, hence a possibility for decay of surface plasmons into bulk plasmons. The coupling need not be

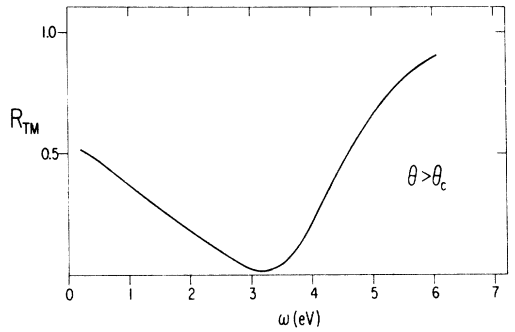

FIG. 7. Surface-plasmon resonance calculated as a function of energy for an angle greater than the prism-spacer critical angle. The full width at half minimum, measured from the asymptotic limit at the low-energy end, is about 2.8 eV.

large for this decay to represent an important contribution to the plasmon lifetime. We assume that ordinary scattering and decay to bulk plasmons occur independently so that the lifetime of a surface plasmon will be

$$1/\tau = 1/\tau_{sp} + 1/\tau_d \ , \tag{16}$$

where τ_{sp} is the surface-plasmon scattering time in the surface zone and τ_d is the inverse of the rate of decay into bulk plasmons. For this decay rate we assume a simple Lorentzian form centered on ω_{sp}.

$$\Gamma_d \equiv 1/\tau_d = \Gamma_{sp}(\tfrac{1}{2}\xi)^2/[(\omega - \omega_{sp})^2 + (\tfrac{1}{2}\xi)^2] \ , \tag{17}$$

and from (16)

$$\tau(\omega) = \tau_{sp}/(1 + \tau_{sp}\Gamma_d) \ . \tag{18}$$

The lifetime of a surface plasmon is thus taken to be energy dependent, being a minimum at ω_{sp}, and increasing to $\tau_{sp} = \tau_b$ far away from ω_{sp}. The parameter values we have used are $\hbar\xi = 0.4$ eV, $\hbar\omega_{sp} = 4.8$ eV, $\Gamma_{sp} = 5\times 10^{15}$ sec^{-1}. Note that when $\omega = \omega_{sp}$, $\tau = 0.31\tau_{sp}$. In this model decay of surface plasmons into bulk plasmons is strongly localized about $\omega = \omega_{sp}$, and the coupling of the modes is weak (even at $\omega = \omega_{sp}$ the rate of decay into bulk plasmons is only about twice the scattering rate). Nevertheless, the surface-plasmon dispersion curve is very sensitive to the existence of nonzero surface-plasmon–bulk-plasmon coupling near $\omega = \omega_{sp}$, and we have not found any model that omits the coupling which will satisfactorily fit the data near $\omega = \omega_{sp}$.

V. COMPARISON OF MODEL CALCULATIONS WITH OBSERVATIONS

In this section we compare our experimental observations of the surface-plasmon dispersion with the predictions of the models described in Sec. IV. We shall also use the available reflectance and ellipsometric data to impose on the model calculations additional constraints and thereby pin down, to the extent now possible, the nature of the conductivity profile at the surface of liquid Hg.

In Figs. 4(a) and 4(b) we display the low-energy portion (1.2–2.7 eV) of the surface-plasmon dispersion curve for liquid Hg. The observed dispersion curve merges smoothly with the light line ($k = n_s\omega/c$) as k decreases, as expected. Although the dispersion curves for the several models also, of course, merge with the light line, the predicted merging occurs at lower energy than that observed. We do not know the origin of this discrepancy, and in the absence of more data the obvious conjectures concerning scattering rate, etc., must remain empty of content.

Figures 5(a), 5(b), and 5(c) display the surface-plasmon dispersion curve for the energy range 2.5–4.5 eV.

Below the asymptotic surface-plasmon excitation energy, which we estimate from these data to be at 4.7 ± 0.2 eV, the SS, LK, and BR model predictions deviate significantly from the observed curve. (In this energy range, the SS and LK dispersion curves are essentially identical, thus describing a limit of sensitivity of the surface-plasmon dispersion curve to surface inhomogeneity.) The GR model prediction provides a much better fit to the experimental data above 2 eV than do the predictions based on the other models. Indeed, on balance, the GR model of the surface transition region leads to a reasonably accurate surface-plasmon dispersion curve over the whole energy range we have studied.

The surface-plasmon dispersion curve bends back towards the light line near $\omega = \omega_{sp}$ by virtue of damping in the electron gas. The BR model dispersion curve will also turn over, but at a much higher frequency than that observed because of the imputed high surface conductivity. The GR model would have a like dispersion curve except for the role of surface-plasmon–bulk-plasmon interaction in increasing the scattering rate near $\omega = \omega_{sp}$. The existence of this interaction is crucial to the fit of the GR model to the observations.

We show, in Fig. 8, a comparison of predicted and observed phase changes on reflection Δ. These data are very precise as no absolute standard is required. The fit generated by the GR model is clearly superior to the fits generated by the other models. In contrast, we show in Fig. 9 that all of the models are deficient with respect to fitting the observed reflectivity ratio ρ, unless the error in the absolute calibration is larger than reported by + 2%. The GR model fit seems slightly

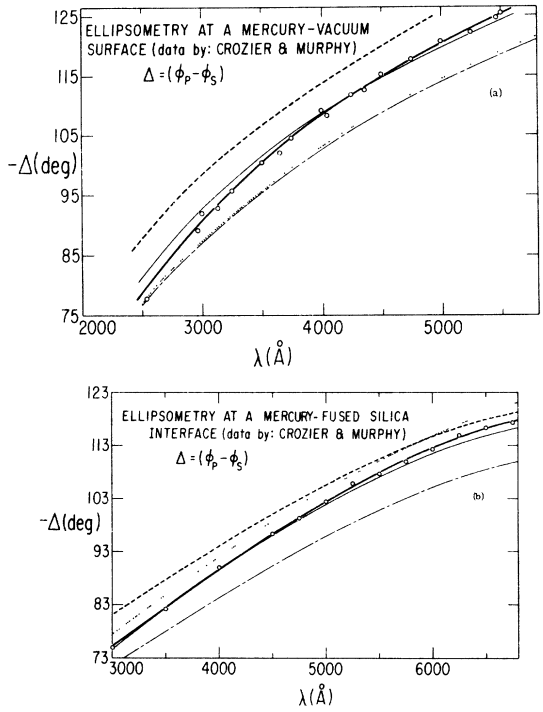

FIG. 8. (a) Comparison of model predictions with the ellipticity obtained directly in an ellipsometric measurement at a free mercury surface, heavy solid line. The Drude sharp surface (SS) and the LK models are shown by the dotted and dash-dotted curves, respectively. The GR and BR behavior is shown by the light solid and dashed curves, respectively. (b) Δ at a mercury-fused silica interface. Same coding as in Fig. 8(a).

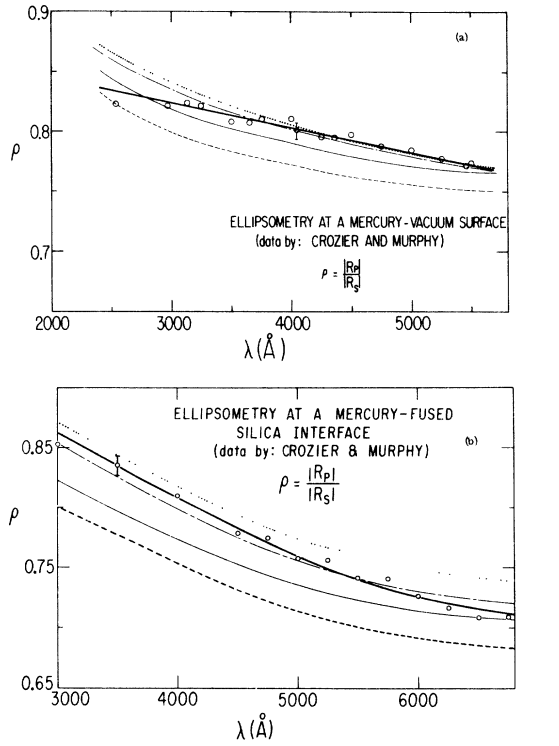

FIG. 9. (a) Ratio of reflection amplitude, directly measured in ellipsometry, for a free mercury surface (heavy solid line). A typical error bar is shown. Also shown is the calculated ratio, as predicted by the four models of the surface. Same coding as in Fig. 8(a). (b) ρ at a mercury-fused silica interface. The curve coding is the same as in Fig. 8(a).

poorer than the others, but not consistently so.

It is interesting to explore how well the various models considered account for the reflection spectrum, i.e., R_s and R_p separately. We note that the BR profile, which accounts well for the "effective optical constants" derived from ellipsometric data via Eqs. (6) and (7), fails to reproduce the values of ρ or Δ from which these "effective optical constants" are derived. This inconsistency arises from the use of the Fresnel relations, i.e., the complete neglect of transition zone effects in reducing the data. In Figs. 10, 11, and 12 we compare the predictions of the several models with measured values of R_s, R_p, and R (unpolarized, near normal incidence). The data in Fig. 10, from Crozier and Murphy,[5] refer to liquid Hg in contact with fused silica, and the angle of incidence is 70°. The GR-model prediction of R_p is somewhat smaller than that observed, as was the prediction of ρ. In contrast, the SS model predicts R_p somewhat higher than observed and, as already stated, the BR-model predictions are a poor fit to the data. All of the models provide a fit to R_s

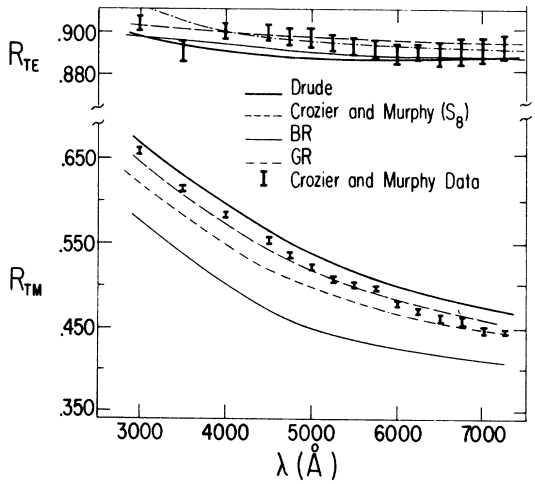

FIG. 10. Oblique reflectivity at a mercury-fused silica interface for the two modes of polarization (after Crozier and Murphy). The angle of incidence is 70°. The predictions of the various models considered in this paper are also displayed. The predictions of LK and SS models are very close and are both represented by the heavy solid line.

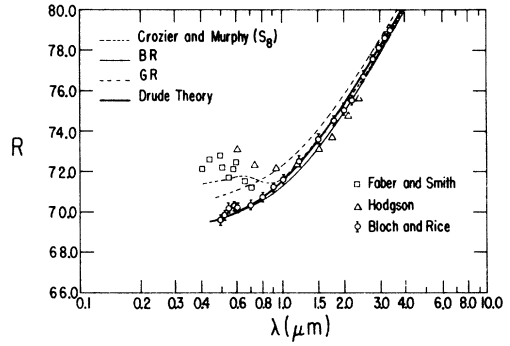

FIG. 11. Normal incidence reflectivity of liquid Hg in contact with a LiF window. The results of Hodgson and Faber and Smith are recalculated to normal incidence using the dielectric function obtained from ellipsometry. The predictions of the four models are also displayed.

within the stated uncertainty of the data. Comparing model predictions with the normal incidence reflectivity, we see that a long wavelengths all models adequately converge to the observed values of the normal incidence reflectivity (Fig. 12). At higher energies, on the other hand, the GR model deviates somewhat from the data shown in Fig. 11.

We have also displayed in Figs. 10–12 the predictions of a modified BR model introduced by Crozier and Murphy and called by them the S_8 model. In this model the conductivity profile (isotropic) is truncated at the metal–fused-silica interface at $z = 3.6$ Å, and the metal-insulator transitions is assumed to occur at $z = 2$ Å, where the dc conductivity is still about 75% of σ_{0max}, the peak conductivity in the transition region. The other profile parameters are $\Delta^b_{S_8} = 3.14$ Å, $\Delta^c_{S_8} = 6.28$ Å, $\tau_s = 1.4\tau_b$, $\sigma_{0s} = 36\sigma_{0b}$ and $\hbar\omega_0 = 0.062$ eV. We note that

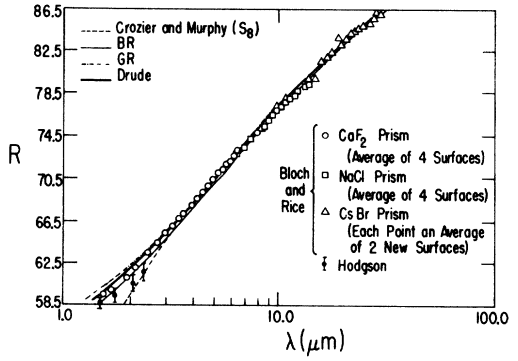

FIG. 12. Model predictions are compared with the infrared normal-incidence reflectivity of liquid Hg in contact with various window materials. The ellipsometric data of Hodgson are recalculated for normal incidence as in Fig. 11.

the S_8 model predicts a too large value for ω_{sp}, just as does the BR model, and that it deviates appreciably from the observed normal incidence reflectance displayed in Fig. 11. The S_8 profile, however, does as well as the GR model in accounting for ρ and Δ, and reproduces the reflectance at 70° incidence very closely.

The GR model is by no means a unique description of the transition region at the liquid-mercury surface. The S_8 profile is very successful in predicting correctly the surface plasmon dispersion curve well below ω_{sp}, the ellipsometric data, and the oblique reflectance. Although the S_8 profile is lacking in its prediction of the normal incidence reflectivity and implies a surface-plasmon frequency much above that observed, inclusion of surface-plasmon–bulk-plasmon interaction, and a rearrangement of the profile parameters, should bring the S_8 model in good agreement with the entire dispersion curve. Furthermore, introduction of anisotropy should lower the peak conductivity of S_8. In fact, within limits, one can fit the available data on liquid Hg with a family of profiles by simply selecting the proper width and peak conductivity and assuming a bulk- and surface-plasmon interaction. The assumption of anisotropic conductivity in the transition region serves to diminish the peak conductivity required.

Finally, we consider the shape of the ATR response function at resonance, i.e., the resonance line shapes. Samples of these are shown in Fig. 13. At high energy, all four models of the transition region lead to a line shape in reasonable agreement with the observed shape, but inaccurately predict the absorption intensity. At low energy, the situation is reversed. Although all four models predict reasonably accurate absorption intensities, the theoretical line shapes are in poor agreement with the observations. In this energy range the widths of the observed resonances in the response function, which measure the imaginary part of the wave vector, are consistently smaller than those predicted. It appears that the intrinsic damping in liquid Hg is smaller than implied in the models considered.

VI. DISCUSSION

Surface plasmons, which may be viewed as charge oscillations localized about and propagating along the surface of a metal, through their interaction with the electromagnetic field, probe a characteristic property of the electron gas which is fundamentally different from that sampled by reflectivity and ellipsometry. The latter measure the interaction of the electromagnetic field with the single electron excitations in the metal. In a

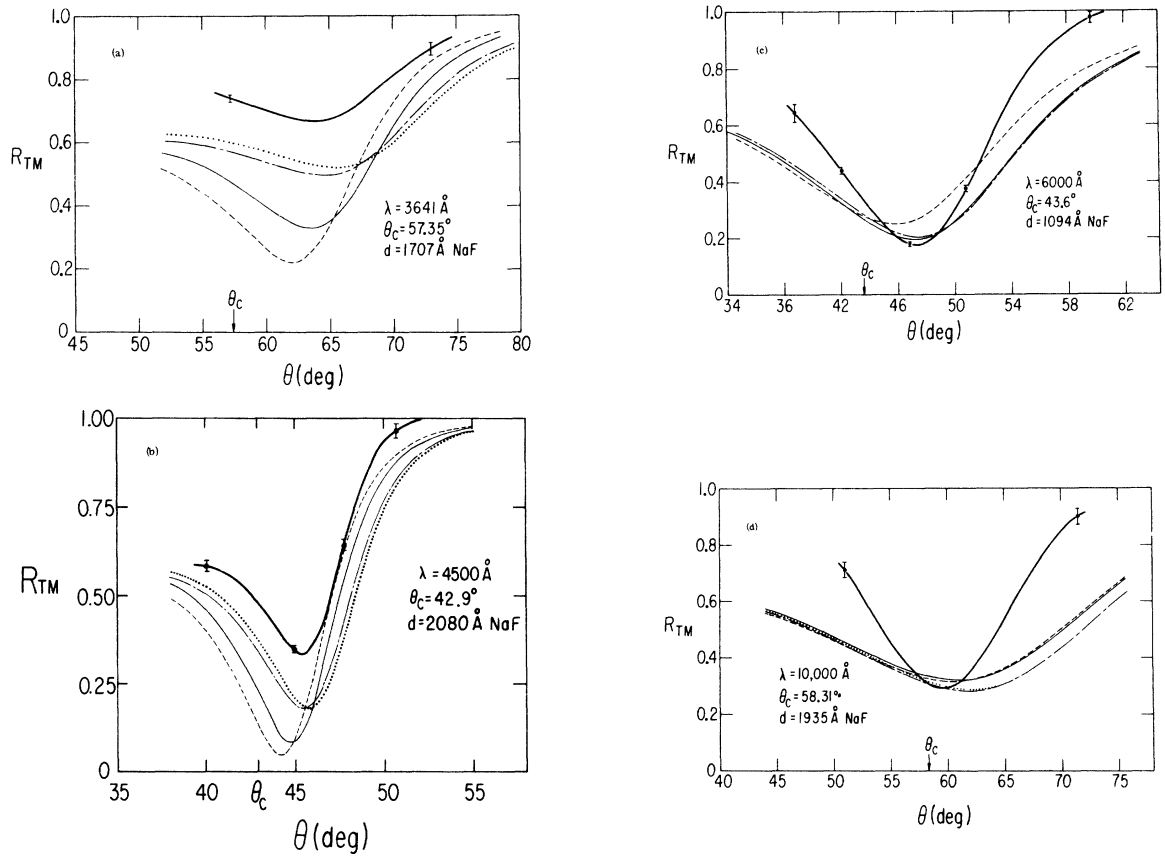

FIG. 13. Line shape for resonance absorption of incident radiation by the surface plasmons. The experimental curve is shown by the heavy solid line on which typical error bars are shown at selected points. The model predictions are also shown and have the coding described in Fig. 8(a).

surface plasmon experiment, however, it is the interaction of collective charge oscillations with the properties of the metal surface, and with the electromagnetic field, which are convoluted in the dispersion curve.

We have studied the properties of liquid mercury primarily because, of the liquid metals, it is the most investigated and additional high-precision data are readily available. From normal incidence reflectance alone one can say very little about the surface. The sharp surface Drude description seems to be adequate. Normal incidence reflectivity, as can be seen from Figs. 11 and 12, is very insensitive to surface structure and a Kramers-Kronig inversion should yield optical constants representative of the bulk. Reflectance of p-polarized light at oblique angles of incidence and ellipsometry are more sensitive to the properties of the transition zone (Figs. 8–10). The surface-plasmon dispersion curve and resonance line shapes supplement this sensitivity and suggest more details about the surface transition region.

The comparison between experimental data for liquid Hg and the predictions of the several models of the surface transition region supports the contentions that: (a) At the surface the conductivity is anisotropic, (b) at the surface the parallel (in plane) component of the conductivity exceeds the bulk conductivity by a factor of order five, and (c) surface-plasmon–bulk-plasmon interaction considerably influences the surface-plasmon dispersion relation.

It would be foolish to contend that the GR model, which incorporates (a), (b), and (c), is a well founded model of the surface transition region; it is, instead, a frankly semiempirical representation. Nevertheless, we believe that characteristics (a), (b), and (c) are robust in the sense that any accounting for the influence of the surface transition zone on the properties of the liquid metal will ultimately include them. Accordingly, we briefly examine the plausibility of (a), (b), and (c) in terms of the electronic and atomic structure of the liquid.

Given that the surface transition region is, by definition, between the bulk liquid and vacuum (or

a dielectric medium), it is not at all unreasonable for the conductivity in that region to have vectorial properties. Whatever the electronic and ionic structure, the transition region is homogeneous in planes parallel to the surface and inhomogeneous along the normal to the surface. Now, from time to time it has been reported that the temperature derivative of the surface tension of liquid Hg is positive,[24-26] indicating that the excess entropy of the surface is negative, which in turn implies that the surface region is somewhat more ordered than is the bulk liquid. While this observation requires confirmation, if accepted it provides weak evidence for the existence of ionic rearrangements in the surface region that likely generate an anisotropic conductivity tensor.

From photoemission studies one can measure the work function of electrons near the surface of a metal. Leaving aside questions of the effect of multiple scattering on the interpretation, it is interesting that photoemission from liquid and crystalline Hg,[27] and from liquid and crystalline In,[27] shows persistence of band-structure effects in the liquid phase. These observations are consistent with the existence of partial ordering of the surface layers of the liquid, but by no means require such an interpretation.

If, indeed, the surface region of liquid Hg is somewhat more ordered than is the bulk, we can expect gross alterations of the electronic transport properties, since in Hg these are extraordinarily sensitive to the ionic structure by virtue of the form of the electron-ion pseudopotential.[28-32] At present there is no way of knowing how "somewhat more ordered" is translated into an ionic configuration. It is worthwhile noting, however, that the dc conductivity of polycrystalline Hg is four times larger than that of liquid Hg,[33,34] and that there are directions in the band structure of crystalline Hg along which the effective mass of the electron is as small as one fifth of the free-electron mass.[35-38] If we accept the existence of Friedel oscillations in the electron density at the surface and the self-consistent ion core rearrangement that must accompany them, the preceding observations suggest that the parallel component of the conductivity in the surface region could plausibly be as large as seven times the bulk conductivity, as in the fit of the GR model to the experimental data. It is important to note that the existence of a large excess surface conductivity does not necessarily imply a corresponding increase in the electron density in the surface region. We suggest that in liquid Hg it is band-structure effects that dominate the change in conductivity, with secondary contributions from changes in scattering time and enhanced electron density.

Finally, although in zeroth-order surface and bulk-plasmon excitations are independent, there are ample possibilities for interaction generated by residual perturbations not considered in the zero-order analysis. It is likely that the indirectly inferred interaction used in the GR model is not a precise measure of the coupling matrix element, but it should be accurate to order of magnitude. The bulk-plasmon–surface-plasmon interaction can be viewed from the point of view of Hopfield's[39] dynamic screening theory. When a surface plasmon wave is excited, the charge fluctuations that occur near the surface give rise to electronic motions which tend to screen out these fluctuations. When the bulk- and surface-plasmon frequencies are sufficiently close, scattering induced line broadening may be sufficient to couple the screening motion of the electrons to the natural frequency of the bulk.

Accepting the concept of a surface transition zone separating bulk liquid from a contact phase, there is no reason to believe that the excess surface conductivity is always positive (surface conductivity exceeds the bulk conductivity). Liquid Hg is, in many ways, not typical of other liquid metals, especially insofar as its electronic transport properties are extraordinarily sensitive to small modifications in local structure. Other metals might have a negative excess conductivity in the surface transition region, and it is likely that for most liquid metals the excess surface conductivity is smaller that in Hg.

ACKNOWLEDGMENTS

We are indebted to Professor E. D. Crozier for making available to us his ellipsometric data on which Figs. 8 and 9 are based. We would also like to thank Dr. John Allan for his critical and stimulating discussions. This research has been supported by a grant from the National Science Foundation (NSF CHE74-08377) and a grant from the Block Board of the University of Chicago. We have also benefitted from the use of facilities provided by the NSF for materials research at the University of Chicago.

APPENDIX: DETAILS OF NUMERICAL CALCULATIONS

The method by which we compute the reflectivity, ellipsometric coefficients, and surface-plasmon dispersion curve of a medium with an inhomogeneous transition region is based on the treatment of the properties of stratified media discussed in considerable detail in Born and Wolf[15] and in Refs. 1 and 10. We will, therefore, only summarize the basic results of this treatment and adapt them to our specific calculations.

The bulk metal is assumed to occupy the half space $z<0$, while the vacuum or contact medium lies in the half space $z>0$. The transition region in the vicinity of $z=0$, is approximated by N homogeneous films of thickness $l \ll L$. The extent of the surface region is characterized by $L=lN$. The density of electrons, dc conductivity, and scattering relaxation time in the ith film are respectively denoted by n_j, σ_{0j}, and τ_j, while the film position is defined by $z_i=z_1+il$. z_1 is the coordinate of the first film and $0 \leq j \leq N$. Within each film the electric and magnetic fields must be consistent with the Maxwell equations with constant n_j, σ_{0j}, τ_j. Furthermore, the tangential components of $\vec{E}$ and $\vec{H}$ must be continuous at the boundary between the ith and $(i+1)$st film. Assuming field dependence of the form

$$\vec{F}(x,z,t)=\vec{F}(z)e^{i(k_x x-\omega t)}, \tag{A1}$$

the Maxwell equations in film i become, for TM polarization,

$$\frac{d^2}{dz^2}H_{yj}-K_j^2 H_{yj}=0, \tag{A2}$$

$$E_{zj}+\frac{ck_x}{\epsilon_j \omega}H_{yj}=0, \tag{A3}$$

$$E_{xj}+\frac{ic}{\epsilon_j \omega}\frac{d}{dz}H_{yj}=0, \tag{A4}$$

and for TE polarization,

$$\frac{d^2}{dz^2}E_{yj}-K_j^2 E_{yj}=0, \tag{A5}$$

$$H_{zj}+\frac{ck_x}{\omega}E_{yj}=0, \tag{A6}$$

$$H_{xj}-\frac{i\omega}{c}\frac{d}{dz}E_{yj}=0, \tag{A7}$$

where $\epsilon_j=\epsilon(z_j,\tau_j,n_j)$ is the dielectric function in the ith film, $K_j^2=k_x^2-\epsilon_j(\omega/c)^2$, $k_x=n_0(\omega/c)\sin\theta$, θ is the angle of incidence, and n_0 is the index of refraction of the vacuum, or the contact medium. The related conductivity is $\sigma_j=\sigma_{0j}/(1+i\omega\tau_j)$, and $\epsilon_j=1+4\pi i(\sigma_j/\omega)$. From a solution of these equations, continued smoothly across each film boundary, one obtains the reflectance amplitudes for the two modes of polarization at a metal-vacuum (dielectric) interface:

$$r_{TM}=\frac{h_0(q_{11}+h_b q_{12})+(q_{21}+h_b q_{22})}{h_0(q_{11}+h_b q_{12})-(q_{21}+h_b q_{22})}, \tag{A8}$$

$$r_{TE}=\frac{g_0(q_{11}+g_b q_{12})+(q_{21}+g_b q_{22})}{g_0(q_{11}+g_b q_{12})-(q_{21}+g_b q_{22})}. \tag{A9}$$

h_0 and h_b are the values of $h_j=iK_j c/\epsilon_j\omega$ in the vacuum (dielectric), and metal bulk respectively. $g_i=-\epsilon_i h_i$ and is similarly defined. $q_{m,n}$ are the matrix elements of the 2×2 matrix $Q=\prod_{j=1}^{N}S_j$. S_i is a matrix which relates the fields just inside the ith film with those just inside the $(i+1)$st film and is given by

$$S_{jTM}=\begin{pmatrix}\cos K_j l & (i/h_j)\sin K_j l\\ ih_j \sin K_j l & \cos K_j l\end{pmatrix}, \tag{A10}$$

$$S_{jTE}=\begin{pmatrix}\cos K_j l & -(i/g_j)\sin K_j l\\ -ig_j \sin K_j l & \cos K_j l\end{pmatrix}. \tag{A11}$$

Thus, while S_i takes us across the ith film, Q takes us through the entire transition region of N films.

For the anisotropic GR model, the following changes are to be affected

$$K_j^2 \to \left[k_x^2\frac{\epsilon_{jx}}{\epsilon_{jz}}-\left(\frac{\omega}{c}\right)^2\epsilon_j x\right],$$

$$h_j \to \frac{icK_j}{\omega\epsilon_{jx}}.$$

The reflectivities are then given by

$$R_{TM}=r_{TM}r_{TM}^*, \tag{A12}$$

$$R_{TE}=r_{TE}r_{TE}^*. \tag{A13}$$

We can rewrite the reflectance amplitude as

$$r_{TM}=|r_{TM}|e^{i\phi_{TM}}, \tag{A14}$$

$$r_{TE}=|r_{TE}|e^{i\phi_{TE}}, \tag{A15}$$

where, as usual,

$$|r|^2=[\mathrm{Re}(r)]^2+[\mathrm{Im}(r)]^2$$

and

$$\phi=\tan^{-1}\frac{\mathrm{Im}(r)}{\mathrm{Re}(r)}.$$

The ellipsometric parameters are then given by

$$\Delta=\phi_{TE}-\phi_{TM}, \tag{A16}$$

$$\rho=\frac{|r_{TM}|}{|r_{TE}|}. \tag{A17}$$

To calculate the surface-plasmon dispersion curve and the absorption line shape we have to include the dielectric spacer as part of the stratified surface transition zone. Then

$$Q'=S_s Q, \tag{A18}$$

where

$$S_s=\begin{pmatrix}\cos K_s d & (i/h_s)\sin K_s d\\ ih_s \sin K_s d & \cos K_s d\end{pmatrix}. \tag{A19}$$

d is the thickness of the spacer and n_s is its index

of refraction. $K_s^2 = k_x^2 - n_s^2(\omega/c)^2$, $h_s = iK_s c/n_s^2\omega$, and $k_x = n_p(\omega/c)\sin\theta_{PS}$. n_p is the prism index of refraction and θ_{PS} is the angle of incidence at the prism-spacer interface. The reflectance amplitude for incident p-polarized light now becomes

$$r'_{TM} = \frac{h_p(q'_{11} + h_b q'_{12}) + (q'_{21} + h_b q'_{22})}{h_p(q'_{11} + h_b q'_{12}) - (q'_{21} + h_b q'_{22})}, \quad \text{(A20)}$$

with "p" referring to the parameters appropriate to the prism. The absorption line shape corresponding to what we measure in our experiment is given directly by

$$R'_{TM} = r'_{TM} r'^{*}_{TM}. \quad \text{(A21)}$$

The corresponding surface plasmon dispersion curve is obtained by plotting $k_{xm}(\omega) = n_p(\omega/c)\sin\theta_m(\omega)$ as a function of $\omega = 2\pi c/\lambda$, where $\theta_m(\omega)$ is the angle at which R'_{TM} is minimum. $\hbar k_{xm}(\omega)$ is in some sense the momentum of the surface-plasmon–radiation-field mixed mode.

In both the LK and GR models we have divided the transition region into 400 slices, each 0.105 Å thick, extending from + 9.135 Å where the electron density is 10^{-9} that of the bulk, to − 32.655 Å, where the Friedel oscillations, though weak still persist and the electron density is 0.999 57 the bulk density.

The BR transition region is divided into 100 slices extending from + 10 Å, where $\sigma_0(z) \sim 10^{-4}\sigma_{0b}$, to − 50 Å. On the vacuum side the slice thickness is 0.2 Å, while on the bulk side, it is 1.0 Å.

The BR profile parameters were determined by Bloch and Rice so as to give the best simultaneous fit to ellipsometrically obtained optical constants, and the normal incidence reflectivity. In the GR model we have fixed the parameters by a best simultaneous fit to the surface-plasmon dispersion curve and the ellipsometric data of Crozier and Murphy.

[1] A. N. Bloch and S. A. Rice, Phys. Rev. 185, 933 (1969).
[2] L. G. Schulz, J. Opt. Soc. Am. 47, 64 (1957).
[3] J. N. Hodgson, Philos. Mag. 4, 189 (1959).
[4] L. G. Lelyuk, I. N. Shklyarenskii, and R. G. Yarovaya, Opt. Spektrosk (USSR) 16, 263 (1964).
[5] E. D. Crozier and E. Murphy, Can. J. Phys. 50, 1914 (1972).
[6] N. D. Lang and W. Kohn, Phys. Rev. B 1, 4555 (1970).
[7] J. C. Slater, *Quantum Theory of Molecules and Solids* (McGraw-Hill, New York, 1963).
[8] D. Guidotti, S. A. Rice, and H. L. Lemberg, Solid State Commun. 15, 113 (1973).
[9] S. A. Rice, D. Guidotti, H. L. Lemberg, W. C. Murphy, and A. N. Bloch, Adv. Chem. Phys. 27, 543 (1974).
[10] H. L. Lemberg, S. A. Rice, and D. Guidotti, Phys. Rev. B 10, 4079 (1974).
[11] A. Otto, Z. Phys. 216, 398 (1968).
[12] B. Fischer, N. M. Marschall, and H. J. Queisser, Surf. Sci. 34, 50 (1972).
[13] I. I. Reshina, Yu. M. Gerbshtein, and D. M. Mirlin, Sov. Phys. Solid State 14, 1104 (1972).
[14] See also references listed in Ref. 9.
[15] M. Born and E. Wolf, *Principles of Optics* (Pergamon, New York, 1965).
[16] O. S. Heavens, *Optical Properties of Thin Films* (Dover, New York, 1966).
[17] The criterion we have used to estimate the surface-plasma frequency from Fig. 5(c) is to compare this with Fig. 14 of Ref. 9, where we displayed the effects of intrinsic damping (excluding radiative damping) on the surface plasma dispersion for a metal with a plasma frequency comparable to that of Hg. From curve III, we notice that the point when the slope is infinite is depressed from the ($k \to \infty$) limit by about 10%. Applying the same construction to Fig. 5(c) we obtain the value 4.7 ± 0.2 eV as the ($k \to \infty$) limit.
[18] E. G. Wilson and S. A. Rice, Phys. Rev. 145, 55 (1966).
[19] A. R. Krauss and R. Gomer, Phys. Rev. (to be published).
[20] R. Alexander, G. S. Kovener, and R. J. Bell, Phys. Rev. Lett. 32, 154 (1974).
[21] E. T. Arakawa, M. W. Williams, R. Hamm, and R. H. Ritchie, Phys. Rev. Lett. 31, 1127 (1973).
[22] J. M. Ziman, Philos. Mag. 6, 1013 (1961).
[23] C. C. Bradley, T. E. Farber, E. G. Wilson, and J. M. Ziman, Philos. Mag. 7, 865 (1962).
[24] D. W. G. White, Trans. AIME 236, 796 (1966).
[25] V. K. Semenchenko, *Surface Phenomena in Metals and Alloys* (Pergamon, Oxford, 1961).
[26] See discussion in Ref. 9.
[27] T. E. Faber, *Introduction to the Theory of Liquid Metals* (Cambridge U.P., London, 1972).
[28] R. W. Shaw Jr. and V. Heine, Phys. Rev. B 5, 1646 (1972).
[29] V. Heine and D. Weaire, *Solid State Physics* (Academic, New York, 1972), Vol. 24.
[30] C. A. Croxton and R. P. Ferrier, J. Phys. C 4, 1909 (1971); 4, 1921 (1971); 4, 2433 (1971); 4, 2447 (1971).
[31] *The Properties of Liquid Metals*, Proceedings of the Second International Conference; Tokyo, Japan, 1972 (Taylor and Francis, London, 1972).
[32] See also discussion in Ref. 9.
[33] A. I. Gubanov, *Quantum Electron Theory of Amorphous Conductors* (Consultants Press, New York, 1965).
[34] *The Properties of Liquid Metals*, Proceedings of the International Conference; Brookhaven National Laboratory, Upton, New York, U.S.A. 1966 (Taylor and Francis, London, 1966).
[35] G. B. Brandt and J. A. Rayne, Phys. Rev. 148, 644 (1966).
[36] S. C. Keeton and T. L. Loucks, Phys. Rev. 152, 548 (1966).
[37] A. E. Dixon and W. R. Daters, Solid State Commun. 3, 377 (1965).
[38] J. M. Dishman and J. A. Rayne, Phys. Rev. 166, 728 (1968).
[39] J. Hopfield, Phys. Rev. 139, A419 (1965).